applied sciences

MDPI

Article

A New Approach for Seepage Parameters Inversion Analysis Using Improved Whale Optimization Algorithm and Support Vector Regression

Haoxuan Li [1], Zhenzhong Shen [1,2,*], Yiqing Sun [1,*], Yijun Wu [1], Liqun Xu [1], Yongkang Shu [1] and Jiacheng Tan [1]

[1] College of Water Conservancy and Hydropower Engineering, Hohai University, Nanjing 210098, China; haoxuanli@hhu.edu.cn (H.L.); wyj6374@csepdi.com (Y.W.); xlq@hhu.edu.cn (L.X.); shuyongkang@hhu.edu.cn (Y.S.); tjccccc@hhu.edu.cn (J.T.)
[2] State Key Laboratory of Hydrology-Water Resources and Hydraulic Engineering, Hohai University, Nanjing 210098, China
* Correspondence: zhzhshen@hhu.edu.cn (Z.S.); syiq417@hhu.edu.cn (Y.S.)

Abstract: Seepage is the primary cause of dam failures. Conducting regular seepage analysis for dams can effectively prevent accidents from occurring. Accurate and rapid determination of seepage parameters is a prerequisite for seepage calculation in hydraulic engineering. The Whale Optimization Algorithm (WOA) was combined with Support Vector Regression (SVR) to invert the hydraulic conductivity. The good point set initialization method, a cosine-based nonlinear convergence factor, the Levy flight strategy, and the Quasi-oppositional learning strategy were employed to improve WOA. The effectiveness and practicality of Improved Whale Optimization Algorithm (IWOA) were evaluated via numerical experiments. As a case study, the seepage parameters of the Dono Dam located on the Baishui River in China were inversed, adopting the proposed inversion model. The calculated seepage field was reasonable, and the relative error between the simulated head and the measured value at each monitoring point was within 2%. This new inversion method is more feasible and accurate than the existing hydraulic conductivity estimation methods.

Keywords: inverse analysis; hydraulic conductivity; Whale Optimization Algorithm; support vector regression

Citation: Li, H.; Shen, Z.; Sun, Y.; Wu, Y.; Xu, L.; Shu, Y.; Tan, J. A New Approach for Seepage Parameters Inversion Analysis Using Improved Whale Optimization Algorithm and Support Vector Regression. *Appl. Sci.* **2023**, *13*, 10479. https://doi.org/10.3390/app131810479

Academic Editor: Andrea Prati

Received: 27 August 2023
Revised: 15 September 2023
Accepted: 18 September 2023
Published: 20 September 2023

1. Introduction

In hydraulic engineering, the seepage parameters of dam materials change with the age of operation. This can lead to a reduction in the structural strength of the dam, triggering serious catastrophes such as dam failure. Seepage analysis based on monitoring data of dams can effectively understand the working condition of dams [1–6]. One of the most important parameters in seepage calculations is the hydraulic conductivity [7]. Currently, there are three methods to determine hydraulic conductivity in hydraulic engineering including the test method, empirical formula method, and back analysis method [8]. The test method can in principle accurately obtain hydraulic conductivity based on in situ sampling. However, indoor and in situ tests are usually subject to large deviations from the actual results due to factors such as short test time, large workload, and discontinuous test time, and the economic costs are generally high. The empirical formula method, based on engineering experience and mathematical assumptions, allows for quick and easy derivation of hydraulic conductivity based on geologic data. However, when applied to complex structures, the results obtained by the empirical formula method are usually inaccurate. Inverse analysis is a method of inverting the hydraulic conductivity of a material based on seepage monitoring data [9–15]. In comparison to the preceding two methods, it is relatively simple to operate, economically inexpensive, and highly reliable. The method is therefore generally applicable to the determination of hydraulic conductivity in seepage calculations. Currently, the inverse analysis method is usually combined with optimization algorithms to accelerate the inversion process.

Artificial intelligence algorithms are gradually introduced into the field of hydraulic engineering [16–21]. Neaupane [22] used Matlab to construct a BP neural network model applied to landslide prediction. Garcia [23] obtained the mapping of transmittance to hydraulic head by ANN. Simpson [24] introduced genetic algorithms in specific inverse problems in geotechnical engineering. Tayfur et al. [25] combined finite elements and artificial neural networks to model a feed-forward three-layer model to invert seepage in an earth and rock dam using backpropagation learning. Saleh [26] obtained reasonable values by combining an artificial neural network and SEEP/W model in calculating the seepage properties of concrete dams.

Support vector machine [27,28] (SVM) is commonly used to solve nonlinear problems. Support vector regression (SVR) [29] is an application of support vector machines when dealing with regression analysis problems and is commonly used to solve small sample regression problems. At the early stage of the development of computer technology, scholars used traditional methods, such as the gradient descent method [30], to improve support vector machines. Such methods generally have some limitations such as low efficiency, high error, and heavy workload. Currently, support vector machines are commonly integrated with artificial intelligence algorithms to solve optimization problems.

In 2016, the Whale Optimization Algorithm (WOA) was proposed by the Australian researcher Mirjalili [31]. The WOA has been applied in hydraulic engineering due to its simple mechanism, few parameters, and strong robustness. Yan et al. [32] employed the WOA to optimize water resource allocation to mitigate the issue of water scarcity. Yang et al. [33] applied an improved binary-coded WOA to formulate the power generation schedule for the Three Gorges Hydropower Station. Banadkooki et al. [34] combined WOA with an integrated machine learning model to achieve groundwater level prediction based on precipitation and temperature data. However, it was also found during the research process that when dealing with complex optimization problems, the convergence accuracy of the standard WOA tends to decrease, and the convergence speed becomes slower. When facing multi-objective optimization problems, the WOA is susceptible to premature convergence. Therefore, it is essential to enhance its performance by optimizing its search strategy.

A lot of research has been conducted to improve the WOA. Kaur et al. [35] combined a variety of chaotic maps to adjust the parameters to improve the performance of WOA. Kaveh et al. [36] introduced a collision body optimization algorithm in WOA, dividing the population into exploratory and mimicry groups to enhance global optimality search capability. Korashy et al. [37] combined the Gray Wolf Algorithm to increase the number of best candidate solutions to improve WOA.

However, there are still some problems in how to avoid local optimization, enhance convergence speed, and improve learning efficiency. The good point set method [38] was introduced as an alternative to the random initial population method to increase the variability within the initial population of whales. A cosine-based nonlinear convergence factor strategy [39] was used to replace the original model of linearly decreasing convergence factor, which balanced the global and local optimization performance. Levy flight strategy [40] and Quasi-oppositional learning strategy [41] were used to avoid premature convergence.

The major contributions of this study are as follows:

1. Three improvement strategies are proposed for the WOA to enhance accuracy and efficiency. The original population initialization method is replaced, the convergence factor is adjusted, and the reverse learning strategy is introduced. These improvement strategies enhance the global search performance and local development performance of WOA from different perspectives.
2. Numerical experiments are conducted to demonstrate the accuracy and effectiveness of the improved whale optimization algorithm (IWOA).

3. SVR is employed to establish a nonlinear mapping relationship between hydraulic head at seepage monitoring points and hydraulic conductivity. By combining IWOA with SVR, a new model for inverting hydraulic conductivity is proposed.
4. The inversion model is applied to the inversion analysis of Dono Dam in Sichuan Province, China. The three-dimensional seepage field and hydraulic head in the dam site area are calculated to verify the accuracy of the parameters obtained from the inversion.

The rest of the paper is organized as follows. In Section 2, we introduced the principle and improvement strategy of the whale optimization algorithm and verified the algorithm's performance with classical test functions. In Section 3, a seepage parameter inversion model combining IWOA and SVR was proposed. In Section 4, the proposed method was applied to an engineering case to invert the target hydraulic conductivity, and simulation results were provided. Section 5 discussed the applicability and limitations of the research results. Finally, conclusions were drawn in Section 6.

2. Improved Whale Optimization Algorithm

2.1. Overview of Whale Optimization Algorithm

The core idea of the Whale Optimization Algorithm (WOA) is to simulate the attacking behavior of humpback whales [42,43], aiming to achieve the optimization solution for the objective function. Whales will engage in continuous communication to select the individual closest to the prey as the current optimal search agent. Other whales will swim towards the prey to surround it to update their search positions. Equations (1) and (2) represent the position update formula for this phase.

$$X(\mathrm{t}+1) = X^*(t) - A \cdot D \tag{1}$$

$$D = |C \cdot X^*(t) - X(t)| \tag{2}$$

Here $X^*(t) = \left(X_1^*, X_2^*, X_3^*, \cdots, X_m^*\right)$ represents the current optimal solution; D represents the distance between the searching individual and the target prey; $X(t)$ represents the position of the other individuals. A and C are determined via Equations (3)–(5).

$$A = 2ar_1 - a \tag{3}$$

$$C = 2r_2 \tag{4}$$

$$a = 2\left(1 - \frac{t}{T_{\max}}\right) \tag{5}$$

where r_1, r_2 represent the random numbers between 0 and 1; a represents a convergence factor; $T_{\max}$ represents the maximum iterations.

The contraction-envelope mechanism and the spiral update mechanism coexist during bubble net attacks. A random probability ω is introduced to discriminatively determine the whale's positional updating pattern. The mathematical model is shown in Equations (6) and (7).

$$X(t+1) = \begin{cases} X^*(t) - A \cdot D & \omega < 0.5 \\ X^*(t) + e^{bl} \cdot D' \cdot \cos(2\pi l) & \omega \geq 0.5 \end{cases} \tag{6}$$

$$D' = |X^*(t) - X(t)| \tag{7}$$

where D' denotes the distance between the current individual and the optimal solution; b represents the spiral shape parameter; l and ω denote random numbers taken from the ranges of -1 to 1 and 0 to 1, respectively.

If $|A| > 1$, the population abandons the current optimal solution and randomly selects a whale as the new optimal solution. The remaining individuals will swim towards this updated optimal solution. Equations (8) and (9) represent the position update formulae for this phase.

$$X(\mathrm{t}+1) = X_{\mathrm{rand}}(t) - A \cdot D \tag{8}$$

$$D = |C \cdot X_{rand}(t) - X(t)| \tag{9}$$

where $X_{rand}(t)$ represents the position vector of the randomly selected whale.

2.2. Improvement Strategies

2.2.1. Initialization of Population Using Good Point Set Strategy

The initial position of the population not only affects the convergence but also determines the precision of the algorithm. WOA usually uses random generation of the initial whale population. This method is poorly robust and prone to uneven distribution of the initial population. To solve this problem, the effective search range is expanded by initializing the population using the good point set method. Assuming that in an s-dimensional Euclidean space there exists a unit cube G_s, the mathematical model that produces the set of good points is shown in Equations (10)–(12).

$$Q_n(m) = \left\{ \left(\left\{ m \cdot r_1^{(n)} \right\}, \left\{ m \cdot r_2^{(n)} \right\}, \cdots, \left\{ m \cdot r_s^{(n)} \right\} \right), 1 \le m \le n \right\} \tag{10}$$

$$\varphi(n) = C(r, \varepsilon) n^{-1+\varepsilon} \tag{11}$$

$$r = \{2\cos(2\pi m/q), 1 \le m \le s\} \tag{12}$$

where $\varphi(n)$ is the deviation between points; $C(r, \varepsilon) n^{-1+\varepsilon}$ represents a constant determined by r and $\varepsilon(\varepsilon > 0)$; q represents the smallest prime number, which satisfies $(q-3)/2 \ge s$.

2.2.2. Cosine-Based Nonlinear Convergence Factors

The convergence factor of standard WOA decreases linearly from 2 to 0. This leads to problems such as slow convergence and low computational accuracy. A nonlinear decreasing formula based on the variation in cosine law is used to regulate the convergence factor. During the initial stages of iterations, it avoids premature convergence of the algorithm. In addition, in the later stage of algorithm iteration, it can improve the local development ability and accelerate the convergence speed. The evolution of the convergence factor with iterations is shown in Figure 1. The expression for a' is shown in Equation (13).

$$a' = \begin{cases} a_{final} + \left(a_{initial} - a_{final} \right) \frac{1 + \left[\cos((t-1)\pi/(T_{\max}-1)) \right]^{\eta}}{2}, t \le \frac{1}{2} T_{\max} \\ a_{final} + \left(a_{initial} - a_{final} \right) \frac{1 - \left[\cos((t-1)\pi/(T_{\max}-1)) \right]^{\eta}}{2}, \frac{1}{2} T_{\max} \le t \le T_{\max} \end{cases} \tag{13}$$

where $T_{\max}$ represents the maximum number of iterations; $a_{initial}$ and a_{final} represent the initial and final values of the improved convergence factor; η is a decreasing exponent between 0 and 1.

2.2.3. Levy Flight Strategy and Quasi-Oppositional Learning Strategy

The whale algorithm sometimes falls into local optimality and fails to converge to a unique solution. Levy flight strategy and Quasi-oppositional learning strategy were introduced to alleviate the trapping in local optima.

Levy Flight is a randomized wandering strategy that focuses on short-range movement with occasional long-range jumping movements. It can randomly wander from any point in any dimension space with any step size, which is helpful to get rid of the local optimal solution. Equation (14) is the position update formula for Levy Flight.

$$R^*_{\mathrm{t}+1} = R^*_{\mathrm{t}} + \lambda \otimes levy(\beta) \tag{14}$$

where λ denotes the step control factor; $levy(\beta)$ is the search path that obeys the Levy distribution, and its search formula is shown in Equation (15).

$$s = \frac{u}{|v|^{\frac{1}{\beta}}} \tag{15}$$

where s represents the randomization step; $\beta = 1.5$; u, v conform to normal distributions, which are $u \sim N\left(0, \sigma_u^2\right), v \sim N\left(0, \sigma_v^2\right)$.

Quasi-oppositional learning strategy is based on the extension of the reverse point concept to produce. In k-dimensional space, assume that there exists a point $P = x(x_1, x_2, \cdots, x_k)$, where $x_i \in [a_i, b_i], i = 1, 2, \cdots, k$, a_i and b_i are the boundary values of the point, the general inverse point OP is expressed as Equation (16).

$$OP = \overline{x}(\overline{x}_1, \overline{x}_2, \cdots, \overline{x}_k) \tag{16}$$

where $\overline{x}_i = a_i + b_i - x_i$. Unlike the ordinary reversal point, the reversal point QOP is a randomly generated point between the ordinary point and the midpoint of the range of values taken by the point. The quasi-opposite number is expressed as Equation (17).

$$QOP = rand\left(\frac{a_i + b_i}{2}, a_i + b_i - x_i\right), i = 1, 2, \cdots, k \tag{17}$$

Levy flight and Quasi-oppositional learning were carried out on whale population, respectively. We took the best whale position after the perturbation and obtained the two best populations. Subsequently, the two populations were merged and ranked by adaptation value. The population with the superior and better adaptation value in the first half was taken as the initial population for the subsequent calculation iteration.

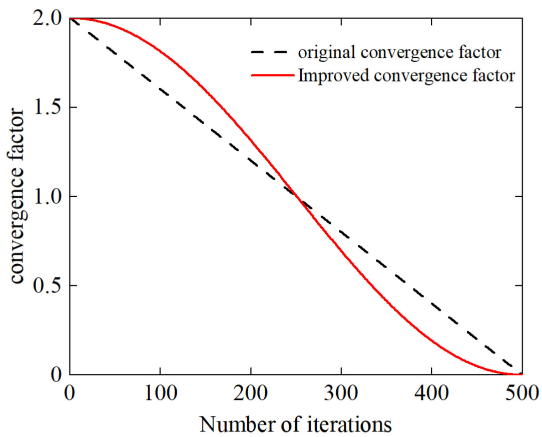

Figure 1. Variation in convergence factors with number of iterations.

2.3. Numerical Experiments on Algorithm Performance

The performance of IWOA needs to be proved by numerical experiments and compared with WOA and other algorithms. Six typical test functions are selected for the experiment to test the algorithm's optimization ability. The mathematical expression, search range, and theoretical minimum value of each test function are shown in Table 1. Sphere, Rosenbrock, and Quartic are single-peak test functions. Single-peak functions, characterized by a solitary extremum, are commonly employed for evaluating the optimization efficiency and search precision of algorithms. Rastrigin, Ackley, and Griewank belong to the category of multi-peak test functions, containing multiple extreme points and frequently employed to assess an algorithm's capacity to get rid of local optima.

Table 1. Test Functions.

Function Name	Mathematical Expression	Search Range	Optimal Solution
Sphere	$F_1(x) = \sum_{i=1}^{n} x_i^2$	$[-100,\ 100]$	0
Rosenbrock	$F_5(x) = \sum_{i=1}^{n-1} \left[100\left(x_i - x_i^2\right)^2 + (x_i - 1)^2\right]$	$[-30,\ 30]$	0
Quartic	$F_6(x) = \sum_{i=1}^{n} i x_i^4 + random[0,1)$	$[-1.28,\ 1.28]$	0
Rastrigin	$F_7(x) = \sum_{i=1}^{n} \left[-x_i^2 - 10\cos(2\pi x_i) + 10\right]$	$[-5.12,\ 5.12]$	0
Ackley	$F_8(x) = -20\exp\left(-0.2\sqrt{\frac{1}{n}\sum_{i=1}^{n} x_i^2}\right) - \exp\left(\frac{1}{n}\sum_{i=1}^{n}\cos(2\pi x_i)\right) + 20 + e$	$[-32,\ 32]$	0
Griewank	$F_9(x) = \frac{1}{4000}\sum_{i=1}^{n} x_i^2 - \prod_{i=1}^{n}\cos\left(\frac{x_i}{\sqrt{i}}\right) + 1$	$[-600,\ 600]$	0

The population size of WOA and IWOA was set to 30, while the number of iterations simulating each test function was fixed at 500. In order to visualize the optimization effect, the iterative process curves of WOA and IWOA for the six test functions are plotted, and the optimization processes of Gray Wolf Optimization (GWO) and Sparrow Search Algorithm (SSA) under the same test conditions are added. Figure 2 presents the convergence process curve.

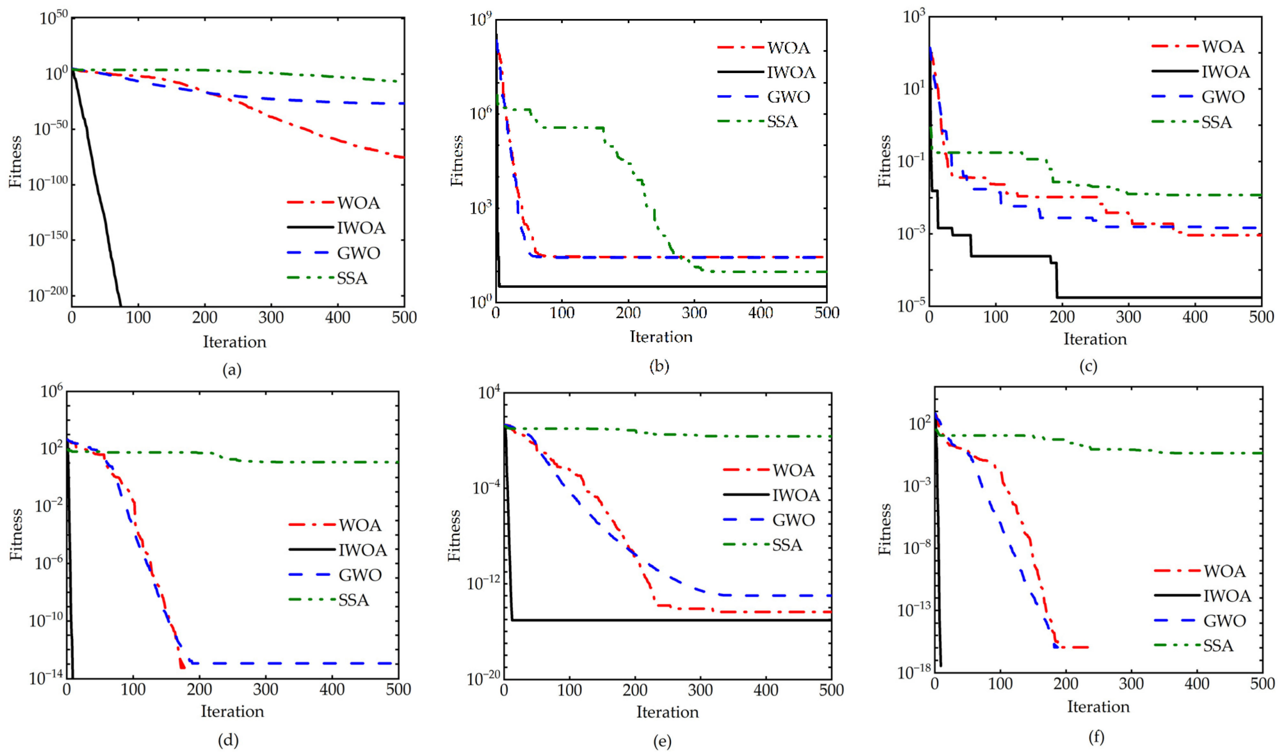

Figure 2. Convergence process curves of test functions: (**a**) Sphere; (**b**) Rosenbrock; (**c**) Quartic; (**d**) Rastrigin; (**e**) Ackley; (**f**) Griewank.

As illustrated in Figure 2, IWOA converges rapidly at the beginning of the iteration. This is attributed to the fact that the good point set method enhances the diversity of the initial whale population, consequently leading to a notable acceleration in the convergence rate. In comparison with the other three swarm intelligence algorithms, IWOA exhibits superior accuracy and convergence speed. These results indicate that the improvement strategies of IWOA are reasonable and effective, and the efficiency and quality of the computation will be greatly improved in the inverse analysis calculation.

3. Seepage Parameters Inverse Model

3.1. Support Vector Regression

SVR has excellent learning ability and generalization ability [44]. It has unique advantages in dealing with nonlinear regression problems. Reasonable parameter combinations were designed within the empirical interval of permeability coefficient values for each material. Each combination of permeability coefficients was substituted into the finite element method calculation to generate the value of the hydraulic head at each monitoring point, which were used as the training sample and the test sample. The nonlinear mapping of hydraulic conductivity to hydraulic head was constructed based on support vector regression.

3.2. Objective Function

To obtain the best estimate of the hydraulic conductivity for each material, the objective function adopts the hydraulic head values. The discrepancy between calculated and measured hydraulic heads should be minimized to the greatest extent possible. The target hydraulic conductivity was obtained by this search process. IWOA was introduced to accelerate the search process. Equation (18) represents the objective function.

$$f = \frac{1}{N}\sum_{i=1}^{N}\left(Y'_i - Y_i\right)^2 \tag{18}$$

where N represents the number of hydraulic head monitoring points; Y_i represents the measured hydraulic head; Y' represents the calculated hydraulic head.

3.3. Procedure of IWOA-SVR Inversion Model

The inversion model procedure can be succinctly outlined through the subsequent steps. Figure 3 illustrates the flowchart of the model.

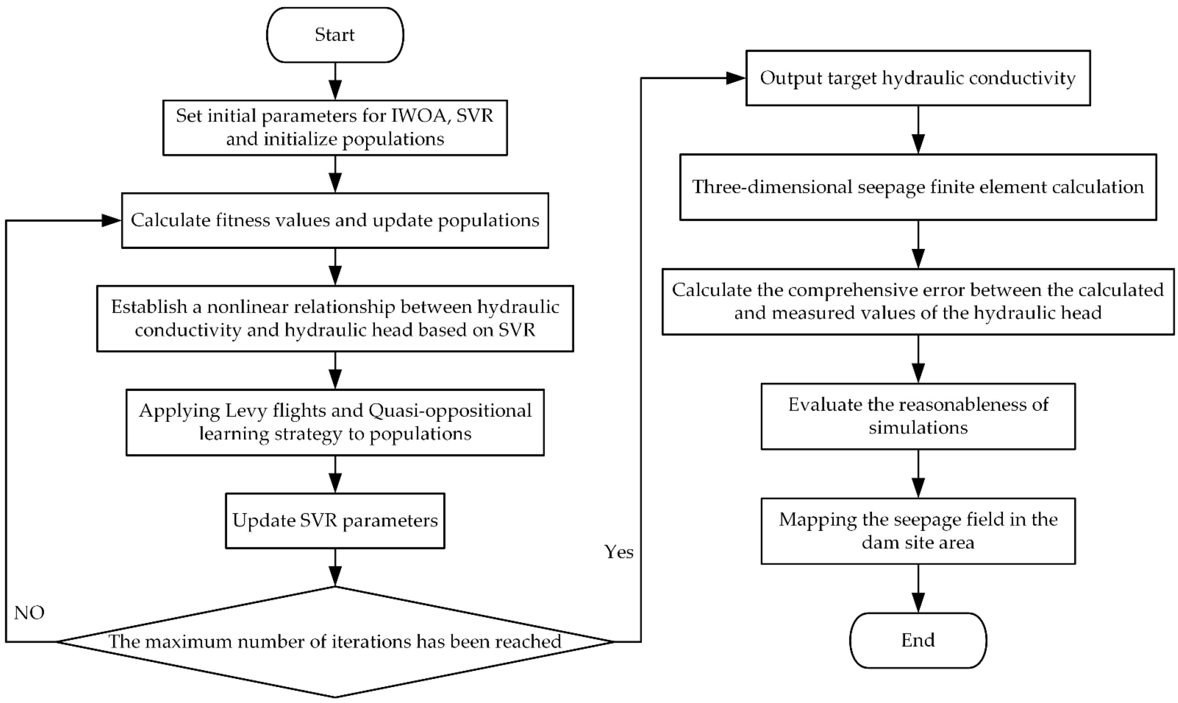

Figure 3. Flowchart of IWOA-SVR inversion model.

Step 1: Inversion analysis model parameter initialization. Set the initialization parameters of IWOA, including basic parameters such as whale population size and iteration number. Set reasonable upper and lower bounds for SVR model penalty parameters and kernel function parameters.

Step 2: Train SVR. A nonlinear mapping between hydraulic conductivity and hydraulic head at monitoring points is established. The parameters of the inversion model are adjusted by IWOA.

Step 3: Test SVR. Take the hydraulic conductivity of the test sample as the input value and the hydraulic head of each monitoring point as the output value to determine whether the accuracy meets the requirements.

Step 4: Update the parameters of IWOA. Update the vectors A, C, the nonlinear convergence factor $a\prime$, the random number l, and the probability ω.

Step 5: Iterative update. Levy flight strategy and Quasi-oppositional learning strategy are performed independently for the current population. The population with higher-ranking fitness values is selected to proceed to the next iteration.

Step 6: Iteration judgment. Determine whether the current iteration has reached the maximum iteration number. If it is reached, output the hydraulic conductivity corresponding to the optimal value of adaptation. Otherwise, skip to step 4.

4. Engineering Example

4.1. Engineering Overview

The Dono Hydropower Station is situated on the Baishui River in Sichuan Province, China. It is a project primarily focused on power generation while also considering downstream ecological water utilization for environmental conservation. Figure 4 shows a site photo of the completed Dono Dam. The concrete panel rockfill dam has a crest elevation of 2374.50 m, a maximum dam height of 108.50 m, a crest width of 10 m, and a normal storage level of 2370.00 m. Figure 5 illustrates the internal material composition of the dam.

Figure 4. Site photo of Dono Dam.

On the right bank of the dam, there are several fractured zones within the mountainous body, containing numerous larger fissures. Groundwater can be quickly discharged into the downstream river. The curtain on the right bank was defective due to poor construction quality, which weakened the curtain's ability to prevent seepage. This resulted in the potential existence of seepage channels on the right bank, thus requiring an inverse study of the hydraulic conductivity of various parts of the right bank within the mountain. Table 2 presents the range of hydraulic conductivity values for each material.

Table 2. Range of hydraulic conductivity for each material.

Materials	Hydraulic Conductivity (m/s)
Q = 5~10 Lu rock layer	1.5×10^{-7}~1.5×10^{-5}
Q = 10~100 Lu rock layer	3.0×10^{-7}~3.0×10^{-5}
Q ≥ 100 Lu rock layer	3.0×10^{-6}~3.0×10^{-4}
Fracture zone	3.0×10^{-6}~1.0×10^{-4}
Defective grout curtain	1.0×10^{-7}~3.0×10^{-6}

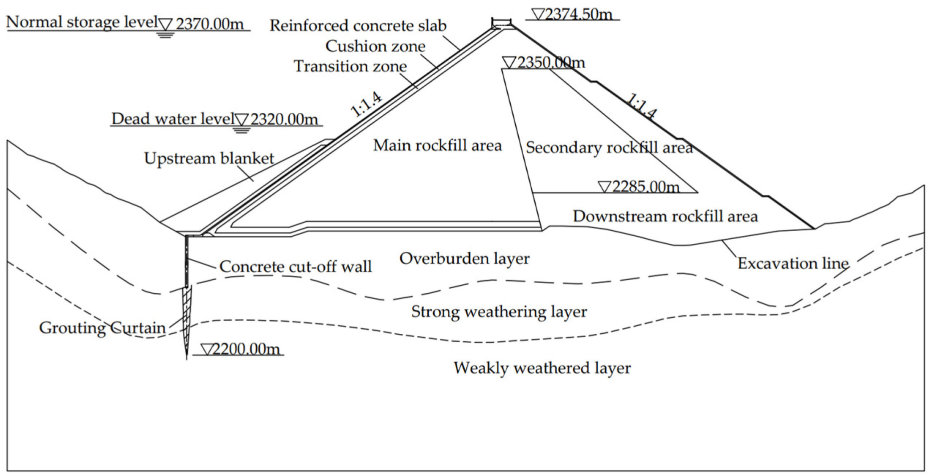

Figure 5. Maximum cross-section.

4.2. Analysis of Monitoring Information

Figure 6 depicts the reservoir water level storage process curve. During the period from 21 October 2021 to 2 November 2021, the reservoir storage level fluctuated between 2369.08 m and 2369.95 m and basically remained stable, so this period was chosen for the inverse modeling.

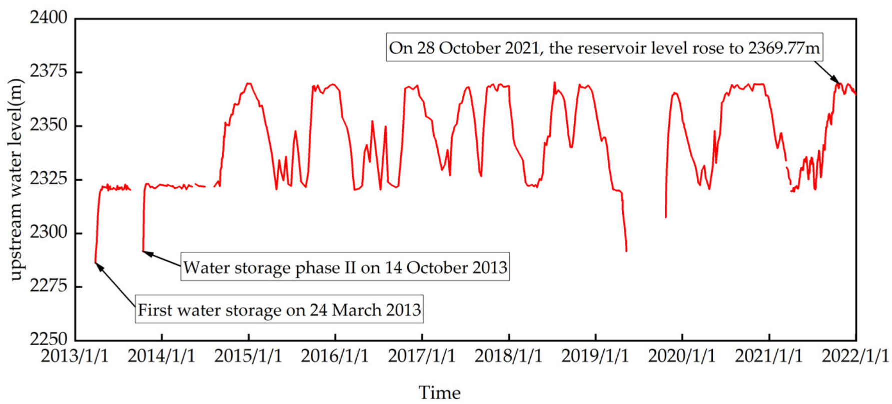

Figure 6. Process line of reservoir level change.

Several seepage monitoring points were installed on the left and right shoulders of the dam. This study aimed to invert the hydraulic conductivities of the poorly impermeable parts on the right bank; therefore, the following inversion process only considers the right bank monitoring data as the basis. Figure 7 presents the installation location of the seepage monitoring points on the right bank.

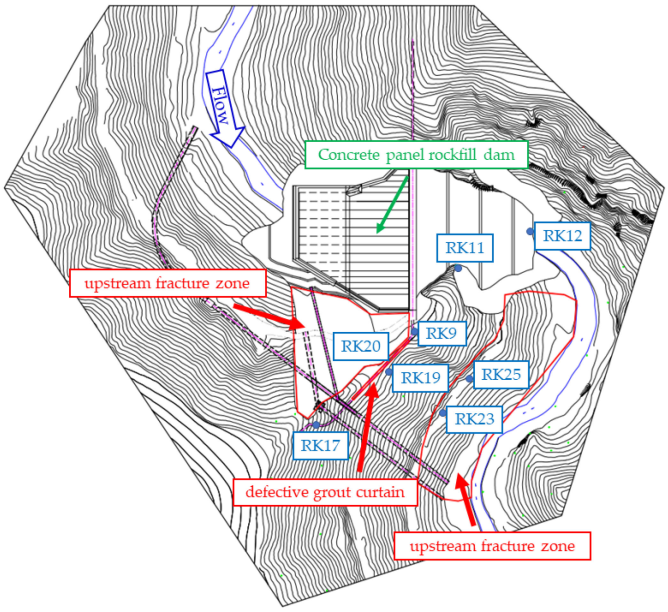

Figure 7. Installation location right bank seepage monitoring points.

4.3. Computation Model

Considering the building boundary and the distribution of rivers in the dam site area, a finite element model was established, as depicted in Figure 8. The X-axis is orthogonal to the dam axis, the Y-axis aligns with the dam axis, and the Z-axis extends vertically upward. The left bank boundary extends approximately 200 m away from the dam, while the right bank boundary extends about 350 m from the dam. The base elevation of the model is 2050 m.

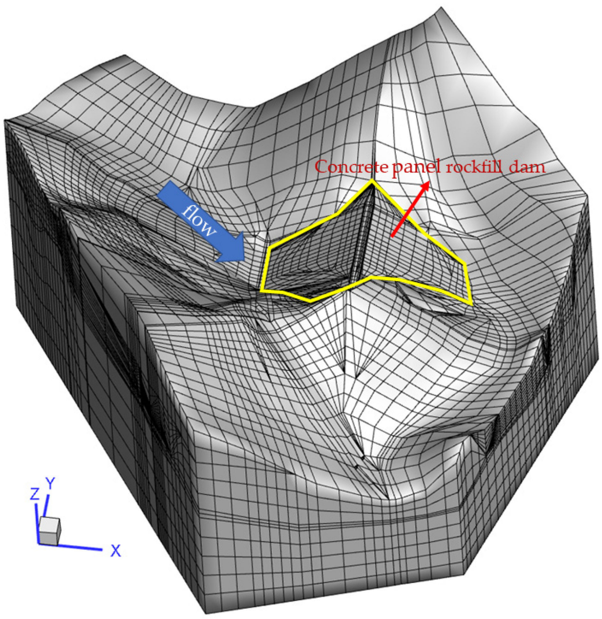

Figure 8. Three-dimensional computational model of the dam.

4.4. Orthogonal Design

During the inversion analysis, excessive construction of training samples may lead to a significant increase in the computational workload for finite element calculations. Orthogonal design (OD) can be a very effective experimental design method to reduce the workload. The OD method was used to arrange the hydraulic conductivity combinations, and the training samples of SVR are constructed by a small number of finite element positive calculations. As shown in Table 3, five uniformly distributed values were taken in the range of values for each of the five hydraulic conductivities mentioned above. These values were then arranged in combinations based on an orthogonal design.

Table 3. Values of each factor based on orthogonal design parameters (m/s).

Materials	Factors	1	2	3	4	5
Q = 5~10 Lu rock layer	1	1.50×10^{-7}	3.86×10^{-6}	7.58×10^{-6}	1.13×10^{-5}	1.50×10^{-5}
Q = 10~100 Lu rock layer	2	3.00×10^{-7}	7.73×10^{-6}	1.52×10^{-5}	2.26×10^{-5}	3.00×10^{-5}
Q ≥ 100 Lu rock layer	3	3.00×10^{-6}	7.73×10^{-5}	1.52×10^{-4}	2.26×10^{-4}	3.00×10^{-4}
Fracture zone	4	3.00×10^{-6}	2.73×10^{-5}	5.15×10^{-5}	7.58×10^{-5}	1.00×10^{-4}
Defective grout curtain	5	1.00×10^{-7}	8.25×10^{-7}	1.55×10^{-6}	2.28×10^{-6}	3.00×10^{-6}

4.5. Simulation Results

4.5.1. Hydraulic Conductivity

Table 4 lists the hydraulic conductivities of the materials determined by the IWOA-SVR inversion model. The hydraulic conductivities obtained from the inversion are within the range of values.

Table 4. Hydraulic conductivity inversion results.

Materials	Search Range	Hydraulic Conductivity (m/s)
Q = 5~10 Lu rock layer	1.5×10^{-7}~1.5×10^{-5}	5.21×10^{-6}
Q = 10~100 Lu rock layer	3.0×10^{-7}~3.0×10^{-5}	2.67×10^{-5}
Q ≥ 100 Lu rock layer	3.0×10^{-6}~3.0×10^{-4}	1.24×10^{-4}
Fracture zone	3.0×10^{-6}~1.0×10^{-4}	9.89×10^{-5}
Defective grout curtain	1.0×10^{-7}~3.0×10^{-6}	1.79×10^{-6}

4.5.2. Hydraulic Head

To confirm the precision of the acquired hydraulic conductivity values, they were applied to conduct seepage calculations. The reliability of the IWOA-SVR inversion analysis model was determined by comparing the calculated hydraulic head values with the measured values. Table 5 presents the absolute and relative errors between the calculated results and the monitored values. The relative error is calculated using Equation (19).

$$e_r = \frac{H_i - H}{\Delta H} \times 100\% \tag{19}$$

where H_i and H, respectively, denote the calculated and measured hydraulic heads. ΔH represents the difference in water level between the upstream and downstream, which is taken as 109.47 m.

Table 5. Errors between measured and calculated hydraulic heads.

Seepage Monitoring Points	Measured Hydraulic Head (m)	Calculated Hydraulic Head (m)	Absolute Error (m)	Relative Error (%)
RK9	2353.15	2352.50	0.65	0.59%
RK11	2273.81	2275.57	−1.76	−1.61%
RK12	2266.68	2264.82	1.86	1.70%
RK17	2351.46	2352.57	−1.11	−1.01%
RK19	2349.40	2348.17	1.23	1.13%
RK20	2362.09	2360.80	1.28	1.17%
RK23	2265.64	2264.28	1.36	1.24%
RK25	2263.08	2265.21	−2.13	−1.94%

As shown in Table 5 and Figure 9, the relative errors between the monitored and calculated hydraulic head values for the eight monitoring points are all within 2%, with

RK25 having the largest relative error of about 1.94%. The results show high accuracy and good stability of the IWOA-SVR inversion analysis model.

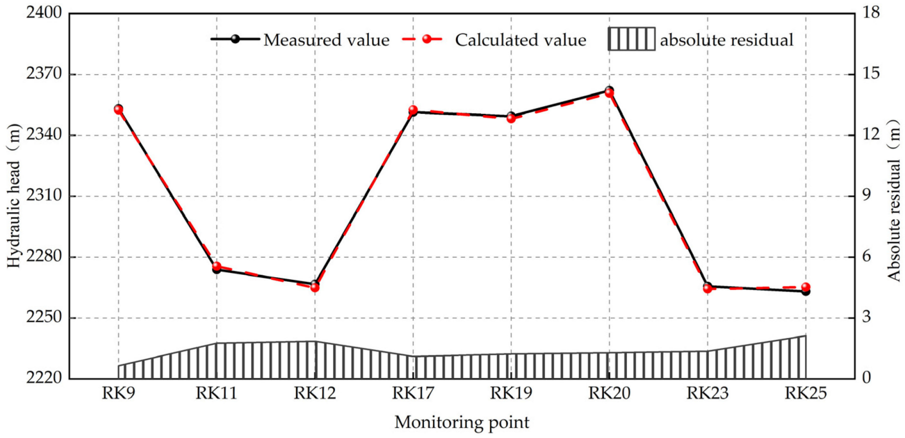

Figure 9. Comparison of calculated and measured hydraulic heads.

4.6. Seepage Field Calculation Results

Figure 10 illustrates the distribution of seepage contours in the dam site area. Reservoir water seeps downstream through the shoulders on both sides of the dam and eventually reaches the downstream river. The hydraulic conductivity within the right bank of the mountain is large compared to the surrounding mountains due to the large number of fissures distributed within the mountain. Therefore, the groundwater can quickly seep to the front of the curtain, making the groundwater level in front of the curtain high. There are many fracture zones in the mountain downstream of the curtain. Groundwater discharges freely through the fracture zones into the downstream channel, and as a result, the water level falls more rapidly. The results are consistent with seepage monitoring data. Therefore, the hydraulic conductivity values obtained by the IWOA-SVR inversion model are reasonable.

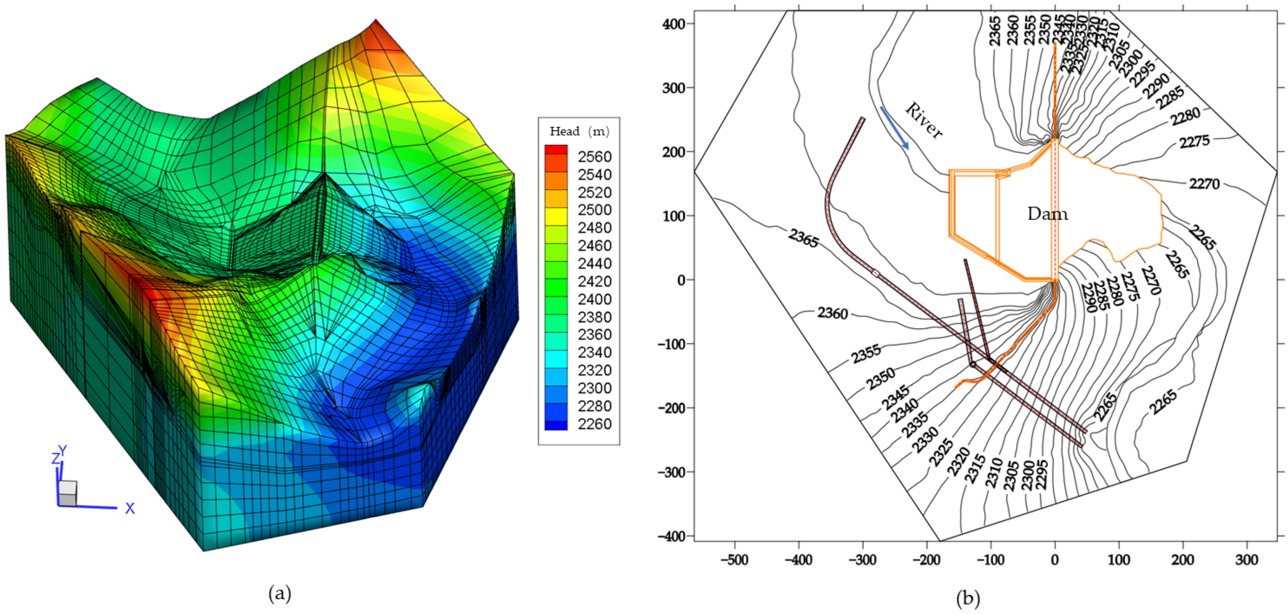

Figure 10. Results of seepage calculations in the dam site area. (**a**) Three-dimensional seepage field of Dono Dam. (**b**) Contour map of groundwater level.

5. Discussion

Concrete panel-faced dams are subjected to high hydraulic head pressures over the long term, causing changes in the hydraulic conductivity of the dam's internal seepage structures and foundation materials as the service life progresses. In seepage analysis calculations, it is essential to employ the actual hydraulic conductivity of the dam materials to ensure the accuracy of the results. In this study, an improved inversion model of seepage parameters was proposed to determine the hydraulic conductivity.

The hydraulic conductivity obtained from the inversion was used for seepage analysis. The three-dimensional seepage field of the dam was reasonable, and the calculated hydraulic head was in good agreement with the monitoring data. The results show that the IWAO-SVR model is feasible for obtaining reasonable hydraulic conductivity.

In this study, a relatively stable water storage period was selected as the inversion period. It can be verified in subsequent studies whether the IWAO-SVR model can accurately invert the hydraulic conductivity of the dam body and dam foundation during upstream and downstream water level changes. In addition, the mechanical parameters of the dam body can be inverted by combining the dam displacement and deformation monitoring data.

6. Conclusions

The Whale Optimization Algorithm was improved and combined with support vector regression to construct an IWOA-SVR seepage parameters inverse analysis model. An inverse analysis of the hydraulic conductivity of various media was carried out based on seepage monitoring data. The hydraulic conductivity values obtained from the inversion were utilized for three-dimensional seepage calculations to obtain the contour map of the groundwater level and hydraulic head, which verified the feasibility of the model. Based on the results of the seepage analysis, the working conditions of the dam can be understood. Subsequently, it can provide a reference for the reinforcement of the weak parts of the seepage control system. The main conclusions are as follows.

(1) The performance of IWOA is improved compared to WOA due to three improvement strategies. The good point set method replaces the random initial population method to expand the search range. The cosine-based nonlinear convergence factor strategy balances search range and search precision. The Levy flight and Quasi-oppositional learning strategy are employed to overcome the local optimum of the algorithm. These three improvement strategies balance the algorithm's global optimization and local development performance.
(2) A new hydraulic conductivity inversion method was proposed by combining IWOA with SVR. Numerical experiments proved that the improvement for IWOA was effective. The IWOA was utilized to search for optimal parameters, while SVR was employed to establish the mapping relationship between hydraulic conductivity and hydraulic head at monitoring points. The IWOA-SVR inversion model was constructed.
(3) The hydraulic conductivity values of target materials were obtained by the IWOA-SVR inversion model. The hydraulic conductivity values were substituted into the finite element model to obtain the hydraulic head at each monitoring point. The maximum absolute and relative errors of the hydraulic heads were -2.13 m and -1.94%. The results show that this inversion model is reliable and can be applied in future engineering calculations.

Author Contributions: Conceptualization, H.L. and L.X.; methodology, Z.S.; software, Y.W.; validation, Y.S. (Yiqing Sun) and H.L.; formal analysis, Y.W.; investigation, J.T. and Y.S. (Yongkang Shu); resources, Z.S.; data curation, Y.S. (Yongkang Shu) and Y.W.; writing—original draft preparation, H.L.; writing—review and editing, J.T. and Y.S. (Yiqing Sun); visualization, H.L. and Y.S. (Yongkang Shu); supervision, Z.S.; project administration, Z.S.; funding acquisition, Z.S. and L.X. All authors have read and agreed to the published version of the manuscript.

Funding: This research was funded by the National Key R&D Program of China (Grant No. 2019YFC1510802) and the National Natural Science Foundation of China (Grant No. 52179130).

Institutional Review Board Statement: Not applicable.

Informed Consent Statement: Not applicable.

Data Availability Statement: Not applicable.

Conflicts of Interest: The authors declare no conflict of interest.

References

1. Jiang, Z.; He, J. Detection Model for Seepage Behavior of Earth Dams Based on Data Mining. *Math. Probl. Eng.* **2018**, *2018*, 8191802. [CrossRef]
2. Liu, M.; Zhong, J.Q.; Rao, X.B.; Liu, J.X.; Wang, W.J. Seepage Monitoring Analysis and Safety Assessment for Yatang Dam. *J. Yangtze River Sci. Res. Inst.* **2007**, *24*, 30–33.
3. Fan, X.F.; Wu, Z.Y.; Liu, L.J.; Wen, Y.F.; Yu, S.; Zhao, Z.P.; Li, Z.F. Analysis of Sluice Foundation Seepage Using Monitoring Data and Numerical Simulation. *Adv. Civ. Eng.* **2019**, *2019*, 2850916.
4. Chu, X.; Xu, M.; Wang, Z. Stability Analysis of Seepage on the Accumulation Dam of a Phosphogypsum Tailings. *J. Eng. Geol.* **2016**, *24*, 661–667.
5. Xu, J.; Wei, W.; Bao, H.; Zhang, K.; Lan, H.; Yan, C.; Sun, W. Failure Models of a Loess Stacked Dam: A Case Study in the Ansai Area (China). *Bull. Eng. Geol. Environ.* **2020**, *79*, 1009–1021. [CrossRef]
6. Strauss, T.; Fan, X.; Sun, S.; Khan, T. Statistical Inversion of Absolute Permeability in Single-Phase Darcy Flow. *Procedia Comput. Sci.* **2015**, *51*, 1188–1197. [CrossRef]
7. Shu, Y.; Shen, Z.; Xu, L.; Duan, J.; Ju, L.; Liu, Q. Inverse Modeling of Seepage Parameters Based on an Improved Gray Wolf Optimizer. *Appl. Sci.* **2022**, *12*, 8519. [CrossRef]
8. Tan, J.; Xu, L.; Zhang, K.; Yang, C. A Biological Immune Mechanism-Based Quantum Pso Algorithm and Its Application in Back Analysis for Seepage Parameters. *Math. Probl. Eng.* **2020**, *2020*, 2191079. [CrossRef]
9. Borazjani, S.; Hemmati, N.; Behr, A.; Genolet, L.; Mahani, H.; Zeinijahromi, A.; Bedrikovetsky, P. Determining Water-Oil Relative Permeability and Capillary Pressure from Steady-State Coreflood Tests. *J. Pet. Sci. Eng.* **2021**, *205*, 108810. [CrossRef]
10. Zhou, C.-B.; Liu, W.; Chen, Y.-F.; Hu, R.; Wei, K. Inverse Modeling of Leakage through a Rockfill Dam Foundation during Its Construction Stage Using Transient Flow Model, Neural Network and Genetic Algorithm. *Eng. Geol.* **2015**, *187*, 183–195. [CrossRef]
11. Virbulis, J.; Bethers, U.; Saks, T.; Sennikovs, J.; Timuhins, A. Hydrogeological Model of the Baltic Artesian Basin. *Hydrogeol. J.* **2013**, *21*, 845–862. [CrossRef]
12. Ren, J.; Shen, Z.-Z.; Yang, J.; Yu, C.-Z. Back Analysis of the 3D Seepage Problem and Its Engineering Applications. *Environ. Earth Sci.* **2016**, *75*, 113. [CrossRef]
13. Chi, S.; Ni, S.; Liu, Z. Back Analysis of the Permeability Coefficient of a High Core Rockfill Dam Based on a RBF Neural Network Optimized Using the Pso Algorithm. *Math. Probl. Eng.* **2015**, *2015*, 124042. [CrossRef]
14. Chegbeleh, L.P.; Akabzaa, T.M.; Akudago, J.A.; Yidana, S.M. Investigation of Critical Hydraulic Gradient and Its Application to the Design and Construction of Bentonite-Grout Curtain. *Environ. Earth Sci.* **2019**, *78*, 370. [CrossRef]
15. Bahrami, A.; Aghamir, F.; Bahrami, M.; Khodaverdiloo, H. Inverse Modeling towards Parameter Estimation of the Nonlinear Soil Hydraulic Functions Using Developed Multistep Outflow Procedure. *J. Hydrol.* **2020**, *590*, 125446. [CrossRef]
16. He, J.; Chen, S.-H.; Shahrour, I. A Revised Solution of Equivalent Permeability Tensor for Discontinuous Fractures. *J. Hydrodyn.* **2012**, *24*, 711–717. [CrossRef]
17. Yu, H.; Wang, X.; Ren, B.; Zeng, T.; Lv, M.; Wang, C. An Efficient Bayesian Inversion Method for Seepage Parameters Using a Data-Driven Error Model and an Ensemble of Surrogates Considering the Interactions between Prediction Performance Indicators. *J. Hydrol.* **2022**, *604*, 127235. [CrossRef]
18. Xu, L.Q.; Li, L. Inversion Analysis of Seepage Parameters Based on Improved Shuffled Frog Leaping Algorithm. *Math. Probl. Eng.* **2021**, *2021*, 6536294. [CrossRef]
19. Shi, Z.; Wu, Z.; Gu, C.; Chen, B.; Zhang, H.; Yin, W.; Wu, B. Calculation Methods for the Permeability Coefficient of Concrete Face Rockfill Dam with Cracks. *Adv. Civ. Eng.* **2019**, *2019*, 6571092. [CrossRef]
20. Zhang, H.; Song, Z.; Peng, P.; Sun, Y.; Ding, Z.; Zhang, X. Research on Seepage Field of Concrete Dam Foundation Based on Artificial Neural Network. *Alex. Eng. J.* **2021**, *60*, 1–14. [CrossRef]
21. Kumar, R.; Pal, S.K.; Gupta, P.K. Water Seepage Mapping in an Underground Coal-Mine Barrier Using Self-Potential and Electrical Resistivity Tomography. *Mine Water Environ.* **2021**, *40*, 622–638. [CrossRef]
22. Neaupane, K.M.; Achet, S.H. Use of Backpropagation Neural Network for Landslide Monitoring: A Case Study in the Higher Himalaya. *Eng. Geol.* **2004**, *74*, 213–226. [CrossRef]
23. Garcia, L.A.; Shigidi, A. Using Neural Networks for Parameter Estimation in Ground Water. *J. Hydrol.* **2006**, *318*, 215–231. [CrossRef]

24. Simpson, A.R.; Priest, S.D. The Application of Genetic Algorithms to Optimisation Problems in Geotechnics. *Comput. Geotech.* **1993**, *15*, 1–19. [CrossRef]
25. Tayfur, G.; Swiatek, D.; Wita, A.; Singh, V.P. Case Study: Finite Element Method and Artificial Neural Network Models for Flow through Jeziorsko Earthfill Dam in Poland. *J. Hydraul. Eng.* **2005**, *131*, 431–440. [CrossRef]
26. Saleh, L.A. Studying the Seepage Phenomena under a Concrete Dam Using Seep/W and Artificial Neural Network Models. In Proceedings of the 2nd International Conference on Engineering Sciences-University-of-Kerbala, Kerbala, Iraq, 26–28 March 2018.
27. Su, H.; Zhang, S.; Wen, Z.; Li, H. Prototype Monitoring Data-Based Analysis of Time-Varying Material Parameters of Dams and Their Foundation with Structural Reinforcement. *Eng. Comput.* **2017**, *33*, 1027–1043. [CrossRef]
28. Su, H.; Wen, Z.; Zhang, S.; Tian, S. Method for Choosing the Optimal Resource in Back-Analysis for Multiple Material Parameters of a Dam and Its Foundation. *J. Comput. Civ. Eng.* **2016**, *30*, 04015060. [CrossRef]
29. Alt, H.W. Numerical Solution of Steady-State Porous Flow Free Boundary Problems. *Numer. Math.* **1980**, *36*, 73–98. [CrossRef]
30. Keerthi, S.S. Efficient Tuning of Svm Hyperparameters Using Radius/Margin Bound and Iterative Algorithms. *IEEE Trans. Neural Networks* **2002**, *13*, 1225–1229. [CrossRef]
31. Mirjalili, S.; Lewis, A. The Whale Optimization Algorithm. *Adv. Eng. Softw.* **2016**, *95*, 51–67. [CrossRef]
32. Yan, Z.; Sha, J.; Liu, B.; Tian, W.; Lu, J. An Ameliorative Whale Optimization Algorithm for Multi-Objective Optimal Allocation of Water Resources in Handan, China. *Water* **2018**, *10*, 87. [CrossRef]
33. Yang, K.; Yang, K. Short-Term Hydro Generation Scheduling of the Three Gorges Hydropower Station Using Improver Binary-Coded Whale Optimization Algorithm. *Water Resour. Manag.* **2021**, *35*, 3771–3790. [CrossRef]
34. Banadkooki, F.B.; Ehteram, M.; Ahmed, A.N.; Teo, F.Y.; Fai, C.M.; Afan, H.A.; Sapitang, M.; El-Shafie, A. Enhancement of Groundwater-Level Prediction Using an Integrated Machine Learning Model Optimized by Whale Algorithm. *Nat. Resour. Res.* **2020**, *29*, 3233–3252. [CrossRef]
35. Kaur, G.; Arora, S. Chaotic Whale Optimization Algorithm. *J. Comput. Des. Eng.* **2018**, *5*, 275–284. [CrossRef]
36. Kaveh, A.; Moghaddam, M.R. A Hybrid Woa-Cbo Algorithm for Construction Site Layout Planning Problem. *Sci. Iran.* **2018**, *25*, 1094–1104. [CrossRef]
37. Korashy, A.; Kamel, S.; Jurado, F.; Youssef, A.-R. Hybrid Whale Optimization Algorithm and Grey Wolf Optimizer Algorithm for Optimal Coordination of Direction Overcurrent Relays. *Electr. Power Compon. Syst.* **2019**, *47*, 644–658. [CrossRef]
38. Liu, X.; Xuan, S.; Liu, F. Artificial Bee Colony Algorithm with Good Point Set and Turn Process of Monkey Algorithm. *Pattern Recognit Artif Intell.* **2015**, *28*, 80–89.
39. Wang, Q.; Wang, M.; Wang, X. Improved Grey Wolf Optimizer with Convergence Factor and Proportional Weight. *Comput. Eng. Appl.* **2019**, *55*, 60.
40. Zhang, Y.; Lu, Z.; Lu, Q.; Wang, J. Research on Optimal Configuration of Photovoltaic Dc Microgrid Based on Levy Flight Improved Bird Swarmalgorithm. *Acta Energiae Solaris Sin.* **2021**, *42*, 214–220.
41. Basu, M. Quasi-Oppositional Differential Evolution for Optimal Reactive Power Dispatch. *Int. J. Electr. Power Energy Syst.* **2016**, *78*, 29–40. [CrossRef]
42. Rana, N.; Abd Latiff, M.S.; Abdulhamid, S.M.; Chiroma, H. Whale Optimization Algorithm: A Systematic Review of Contemporary Applications, Modifications and Developments. *Neural Comput. Appl.* **2020**, *32*, 16245–16277. [CrossRef]
43. Rana, N.; Abd Latiff, M.S.; Abdulhamid, S.M.; Misra, S. A Hybrid Whale Optimization Algorithm with Differential Evolution Optimization for Multi-Objective Virtual Machine Scheduling in Cloud Computing. *Eng. Optim.* **2022**, *54*, 1999–2016. [CrossRef]
44. Byun, H.; Lee, S.W. A Survey on Pattern Recognition Applications of Support Vector Machines. *Int. J. Pattern Recognit. Artif. Intell.* **2003**, *17*, 459–486. [CrossRef]